npj | biological physics and mechanics

Article

https://doi.org/10.1038/s44341-025-00028-0

Long-term physiological flow rescues regressed microvascular networks and increases their longevity

Marie Floryan[1], Elena Cambria[2], Adriana Blazeski[1], Mark F. Coughlin[2], Zhengpeng Wan[2], Giovanni Offeddu[2], Vinayak Vinayak[3,4], Aayush Kant[3,4], Jordan Whisler[1], Vivek Shenoy[3,4] & Roger D. Kamm[1,2] ✉

The incorporation of a functional perfusable microvascular network (MVN) is a common requirement for most organ on-chip-models. Long-term perfusion of MVNs is often required for the maturation of organ phenotypes and disease pathologies and to model the transport of cells and drugs entering organs. Here, we use a microfluidic pump to apply continuous, recirculating physiological flow through self-assembler microvascular networks. In our microphysiological system (MPS), we observe that flow can recover perfusion in regressed MVNs and maintain perfusable MVNs for at least 51 days. Throughout the 51 days, however, the MVNs are continuously remodeling to align with the direction of bulk flow and only appear to attain morphological homeostasis with the use of maintenance medium without growth factors. We observed that the flow resistance of the MVNs decreases over time, and using a computational model, we show that stable vessels have higher flow rates and velocities compared to regressing vessels. Cytokine analysis suggests that static conditions generate an inflammatory state, and that continuous flow reduces inflammation over an extended period. Finally, through bulk RNA sequencing we identify that both the endothelial and fibroblast cells are actively engaged in flow-induced vascular and matrix remodeling and that these effects persist for at least 2 weeks. This MPS can be applied to study hemodynamically driven processes, such as metastatic dissemination or drug distribution, or to model long-term diseases previously not captured by MPS, such as chronic inflammation or aging-associated diseases.

Incorporating continuously perfused 3D microvascular networks (MVNs) within microphysiological systems (MPS) is critical to developing novel models of disease. While the capabilities of MPS in modeling diseases have significantly expanded in recent years, there is a need to develop new vascularized MPS that allow for continuous monitoring of hemodynamic processes such as drug transport or cancer metastatic dissemination, and that capture long-term disease dynamics central to age-related cellular changes, chronic diseases, or inflammatory processes. In each case, the value of the MPS is enhanced by closely mimicking physiological flow conditions and the morphology of the organ's specific microvascular bed. Local changes in blood flow dynamics, dictated by changing vascular morphology, are often associated with disease states, such as inflammation[1]. In the case of cancer, the inflammatory state of the endothelium is crucial as it influences immune or tumor cell adhesion, their retention at the site of adhesion, and their transendothelial migration. Furthermore, inflammation may also affect MVNs. Inflammation promotes angiogenesis, EC proliferation and migration, increases vascular permeability, and facilitates extracellular matrix (ECM) remodeling[2,3]. Capturing the inflammatory state of the endothelium is therefore critical for modeling the immune response. Continuous perfusion of MVNs is a promising approach to meet the requirements of capturing hemodynamic processes and long-term disease dynamics.

MPS that incorporate self-assembled MVNs are an attractive approach to modeling such dynamics because their morphology closely mimics that of the in vivo microcirculation. Such MVNs typically form over 4 to 7 days and are grown statically for up to 14 days before regression sets in refs. 4,5. This

[1]Department of Mechanical Engineering, Massachusetts Institute of Technology, Cambridge, MA, USA. [2]Department of Biological Engineering, Massachusetts Institute of Technology, Cambridge, MA, USA. [3]Center for Engineering Mechanobiology, University of Pennsylvania, Philadelphia, PA, USA. [4]Department of Materials Science and Engineering, University of Pennsylvania, Philadelphia, PA, USA. ✉e-mail: rdkamm@mit.edu

culture period has enabled numerous important studies: circulating immune cells have been introduced to investigate the role they play in various diseases, notably metastatic cancer[6–8], and the subcutaneous absorption of drugs has been characterized[7]. These studies, however, lack the incorporation of hemodynamics.

Most MPS studies incorporating continuous perfusion of MVNs have limited their perfusion periods to 24-h to 7 days (up to 14 days total)[9–11]. Luminal flow conditioning over two days was shown to have anti-inflammatory effects[10], and in a similar microfluidic device, luminal flow was shown to promote the longevity of placental MVNs for up to 14 days[9]. Moreover, the magnitude of flow rate and its corresponding velocity and wall shear stress (WSS) were shown to influence vascular diameters[12]. Static culture and low flow perfusion of MVNs resulted in regression and decreases in vascular diameters over 14 days[9], while relatively high flow supplied by a microfluidic pump resulted in increases in vascular diameters over two days of continuous perfusion[11]. Although these studies have provided important insights into the application of relatively short-term flow, a detailed characterization of the effect of long-term (>14 days) physiological luminal flow on the morphology and function of MVNs is currently missing.

Here we present an MPS with 3D MVNs perfused with a microfluidic pump for 51 days and note several important phenomena. Continuous flow recovers perfusion of regressed vessels, and in perfusing initially healthy vessels, we observe long-term (weeks) remodeling of the MVNs. Computational modeling of the MVNs provides insights into determining how individual vessel segments will remodel. Furthermore, long-term flow is shown to reduce inflammation of the MVNs. Finally, bulk transcriptomic analysis reveals governing pathways in the remodeling MVNs. The full characterization of this long-term, continuously perfused MPS provides insights into vascular responses to flow in engineered platforms and can be used to study long-term diseases and to incorporate aspects of hemodynamic processes previously not captured by MPS.

Results

Physiological flow rescues perfusion in regressed vessels

Vascular networks grown under static conditions begin to regress after about 14 days in culture and are therefore of limited use for long-term experiments. To address this, we examined the ability of physiological flow to recover networks that were on the verge of losing perfusability. MVNs were grown in a previously described device[11] and flow was provided by a microfluidic pump[13] to introduce flow at a specified time (Fig. 1a–c). The pulsatility index, which is the difference between the maximum and minimum velocities divided by the average velocity, of the steady state flow was 0.30 (Fig. 1d), comparable to the in vivo pulsatility index of cerebral mouse microcirculation[14]. Notably, the pump input pressure was held constant at 6 kPa for all flow experiments, which yielded the flow rates and pressure drops shown in Supplementary Fig. 1. In brief, the flow rate was <10 μL/min and increased to ~140 μL/min as the hydraulic resistance of the MVNs decreased, which corresponds roughly to a pressure difference of ~1000 Pa and decreasing to ~250 Pa. Network morphology, perfusability, and permeability were chosen as the three key features that could be compared directly to *in vivo* microcirculation.

Visually, MVNs under static conditions were fully formed and interconnected on day 7 (Fig. 2a) and then began to narrow, lose connections and, ultimately, cease to be perfusable (Fig. 2a). Under static conditions, most MVNs were perfusable by day 7 but then regressed and lost perfusion

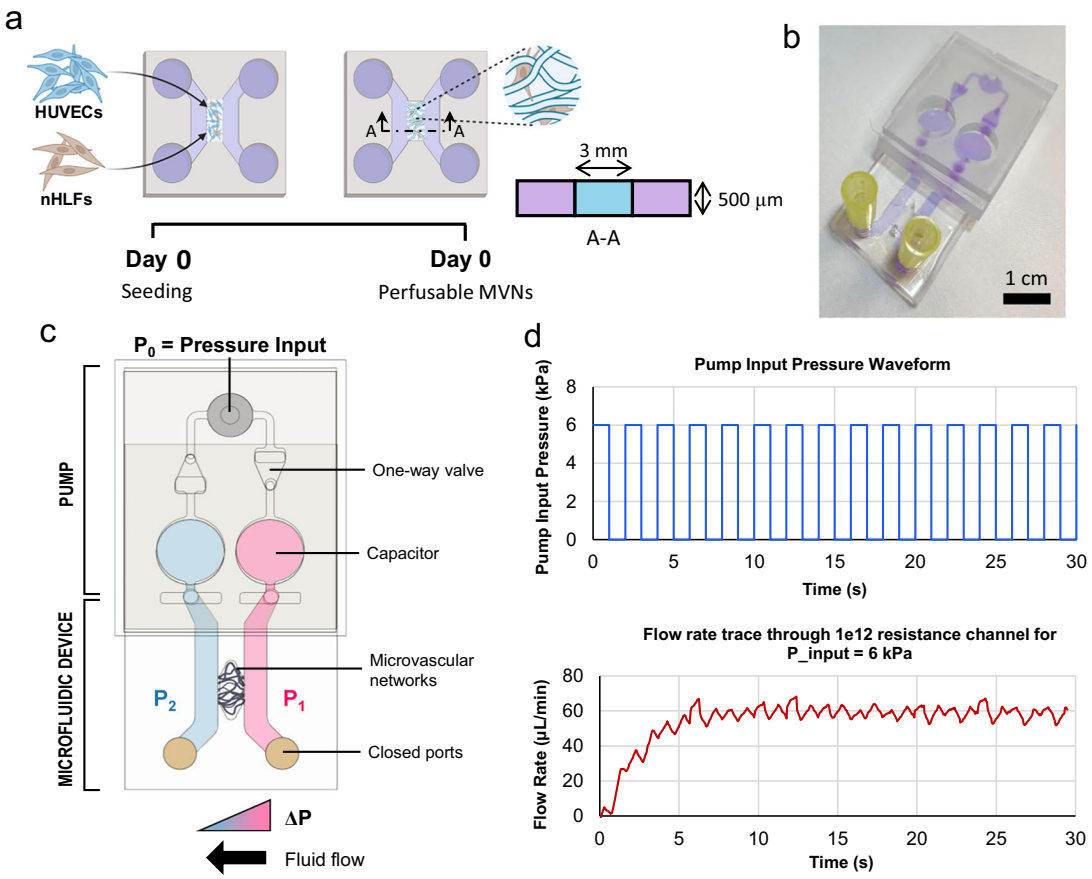

Fig. 1 | Experimental timeline and setup used for pump flow experiments. a The timeline for seeding and MVN formation in a microfluidic device. **b** A microfluidic pump is attached to the microfluidic device to introduce flow. **c** The pump generates recirculating flow by a pressure drop across the microvascular networks. Pump components are labeled. **d** The input pressure profile to the pump oscillates between a user-defined peak pressure and atmospheric pressure at a user-defined frequency. The corresponding bulk flow rate (trace is a moving average over 250 ms) quickly reaches steady flow within seconds of the input pressure commencing.

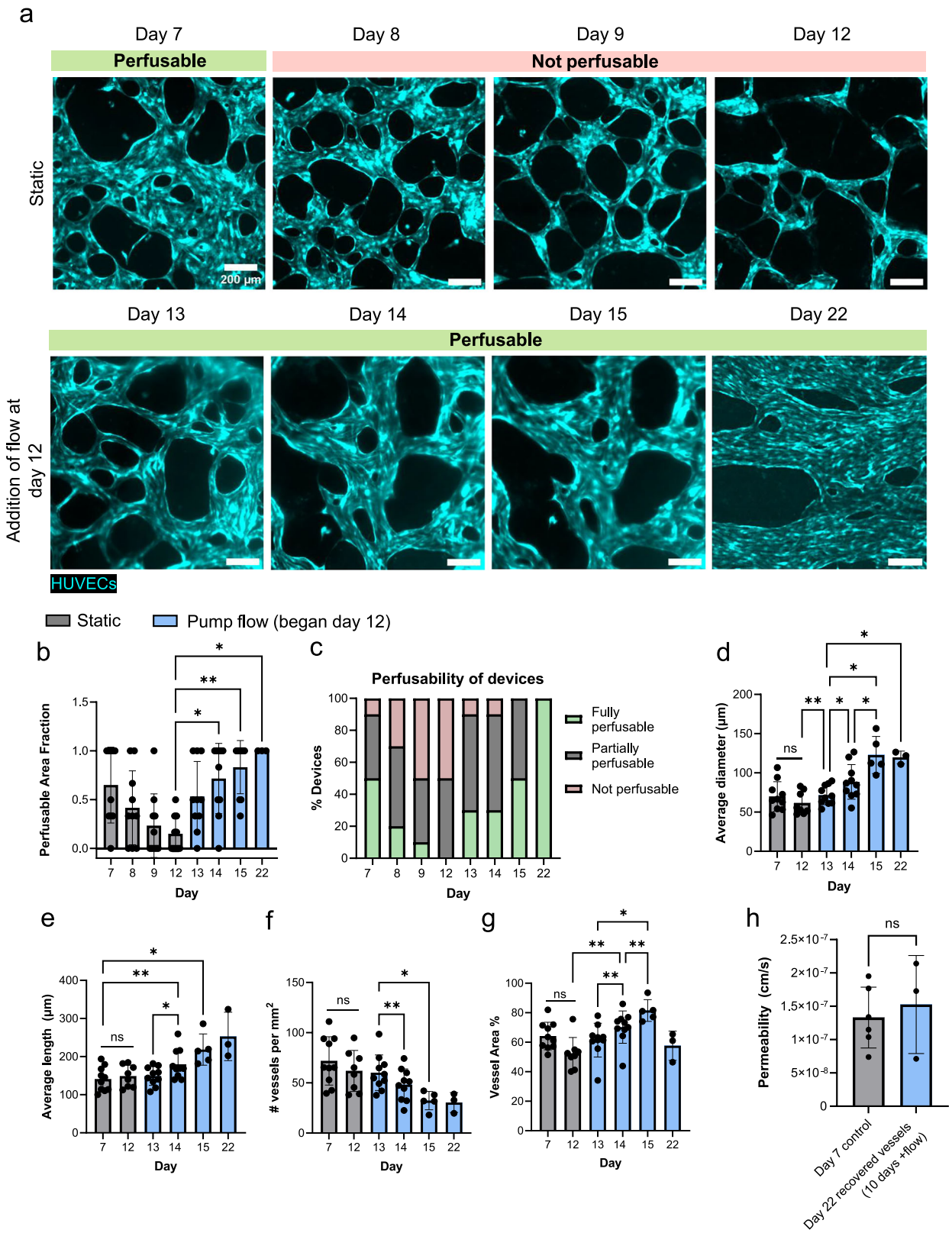

Fig. 2 | Flow can rescue perfusion in regressed vessels. a Images of the same vascular bed over time. Scale bar is 200 µm. **b** The perfusable area fraction of devices and **c** the collective perfusability of MVNs is reported. The average vessel diameter (**d**), length (**e**), vessel density (**f**), and vessel area (**g**) are reported. **h** The permeability of the recovered vessels on day 22 and control vessels on day 7 were measured. $n = 3–10$ MVNs.

by day 12 (Fig. 2a–c). Flow commenced on day 12 and by day 15 the perfusable network fraction significantly increased compared to day 12 (Fig. 2a–c). MVN regression was heterogeneous. While Fig. 2a shows one scenario, where MVNs were initially perfusable and rapidly lost perfusability by day 8, other MVNs that were not perfusable on day 7 and continued to regress through day 12 also demonstrated recovery of perfusability within 24 h of initiating flow (Supplementary Fig. 2). In other cases, MVNs remained partially perfusable through day 12 (Fig. 2b, c). During the

regression period (days 7–12), no differences in average MVN morphology were observed, likely due to measuring the average of the morphological features (Fig. 2d–g). During the subsequent flow period (days 12–22), the average diameter (Fig. 2d) and average length (Fig. 2e) increased, the vascular density decreased (Fig. 2f), and the vessel projected area (projected onto the x-y plane) increased until day 15 (Fig. 2g). The initial increase and subsequent decrease in vessel projected area (Fig. 2g), may be explained by vessel pruning, where vessels initially increase in diameter upon flow commencing, leading to an increase in projected vessel area, vessel pruning reduces the number of vessels (Fig. 2f) ultimately resulting in a decrease of the projected vessel area. The permeability of the recovered MVNs on day 22 (10 days with flow) was comparable to MVNs on day 7 (Fig. 2h). Furthermore, the perfusability of MVNs seeded in a high concentration of fibrinogen (5 mg/mL) (high fibrinogen MVNs) was also rescued by flow (Supplementary Fig. 3). While the high fibrinogen MVNs initially appeared less connected and had smaller radii compared to control MVNs (3 mg/mL fibrinogen), after 6 days of flow the high fibrinogen MVNs were fully perfusable, visually appeared similar and exhibited no significant differences in morphological parameters, with the exception of vessel area coverage that was reduced by ~ one third compared to control MVNs (Supplementary Fig 3). These results demonstrate that *in vitro* vascular networks can be rescued up to, and even beyond the time at which they lose perfusability. Thereafter, remodeling continues while vascular permeability remains relatively constant.

Luminal flow increases the longevity of MVNs

Next, the question of how long the effects of flow can maintain barrier integrity was addressed. For all subsequent experiments, flow commenced on day 7. Application of flow to the MVNs was observed to increase their longevity but the resulting MVNs progressively grew in diameter, eventually failing to resemble in vivo vasculature (Fig. 3a). Reasoning that the continued presence of growth factors in the media could be partly responsible, new experiments were performed with different media compositions. The supplemental growth factors present in growth medium were ultimately found to play a role in the morphological remodeling of the MVNs in response to flow and growth factors, leading to the uncontrolled growth (Fig. 3a). To counteract this, medium without the supplemental growth factors, termed maintenance medium from here on, was used and the MVNs were found to be perfusable for 51 days when experiments were terminated, though the system could have persisted for longer time (Fig. 3a). Conversely, MVNs cultured with maintenance medium under static conditions regressed and lost perfusion by day 12 (Supplementary Fig. 4), similar to culture with regular growth medium under static conditions. In view of these findings, all subsequent flow experiments used growth medium for the first 7 days during vessel growth and were transitioned to maintenance medium from the time that flow was started on day 7 unless otherwise specified.

Under these conditions, despite improved stability, the MVNs continued to undergo remodeling over the course of 51 days (Fig. 3a, bottom row). Prior to commencing flow, smaller vessel radii were predominated, but as the MVNs remodeled due to flow, the distribution of vessel radii increased to be nearly uniform by day 51, at which time large and small vessel radii were similarly likely to be present (Fig. 3b). (Note that, at all time points, there was a spurious peak in the distributions at large radii; this was an artifact of the segmentation and skeletonization algorithm used that sets a limit on the maximum allowable vessel radius to avoid erroneous measurements.) Similarly, while the distribution of vessel lengths followed a truncated Gaussian distribution with a bias towards shorter vessels prior to flow, with time the distribution flattened and broadened until day 51, where long vessels were equally likely to be present as short vessels (Fig. 3b). During the 44 days of flow, the average vessel diameter increased ~3-fold (Fig. 3c) and the average vessel length increased ~4-fold (Fig. 3d). The vascular density sharply declined in the first two weeks of flow, and by day 51 there was an 11-fold reduction compared to day 7 (Fig. 3e). The area occupied by the vessels declined in the first week of flow and then remained steady (Fig. 3f). Despite the continued changes in the average of the vessel morphology parameters, the main flow paths were already apparent by day 24 (Supplementary Fig. 5). Notably, vessel orientation changed dramatically over time with continuous flow (Fig. 3g). From day 7 to 15, vessels had little directional orientation, but by day 51, most vessels became aligned with the direction of the pressure drop across the MVNs, due to a combination of regression of vessels perpendicular to the overall pressure gradient and persistence and growth of those parallel to it. The sum of the vessel lengths exhibited this same trend but also demonstrated a large degree of vascular pruning with a dramatic reduction overall in vascular lengths (Fig. 3h). For both probability and sum of vessel lengths cases, only small differences were noted between days 7 and 16, but by day 51 most of the MVN length was oriented in the direction of the pressure drop across the MVNs. These results indicate significant directional remodeling between days 16 and 51. Thus, while the rate of change in vascular morphology slowed over time, some changes continued even through day 51, suggesting that the MVNs remained dynamic.

Changes in the functionality of the vascular networks were also evaluated. Permeability values were found to remain low between days 7 and 31, ranging between 1×10^{-7} cm/s and 3×10^{-7} cm/s for a 70 kDa FITC-dextran (Fig. 3 i, Supplementary Fig. 6), on the order of previously reported values[10]. Notably, the variability in permeability lessened over time, suggesting that the networks were functioning more uniformly. The hydraulic resistance of the MVNs, which is the resistance to fluid flow and calculated following an analytical relationship (Supplementary Fig. 7), was ~1×10^{13} Pa•s•m^{-3} on day 7 when the networks first became fully perfusable, then proceeded to decrease during one week of flow as the diameters of the largest vessels increased, and then remained stable between 1×10^{11} and 1×10^{12} Pa•s•m^{-3} through day 22 (Fig. 3j). Cell-cell junctions, evaluated through immunofluorescence staining of VE-cadherin, remained intact between days 7 and 14 (Supplementary Fig. 8). Furthermore, live/dead staining indicated the MVNs were mostly composed of live cells at days 7 and 14 (Supplementary Fig. 9). Luminal flow therefore prolongs the life of MVNs and leads the MVNs to morphologically remodel while maintaining low values of permeability.

Unidirectional flow maintains vascular perfusability better than flow with alternating direction

Intravascular flow is widely recognized as exerting a strong influence on network morphology and function. To explore this further, the effect of flow with alternating direction was examined as used in previously reported experiments incorporating hydrostatic pressure to generate flows on a rocker platform (Supplementary Fig. 10a)[15]. Three conditions were compared: 1) MVNs with rocker flow and with growth medium, 2) MVNs with rocker flow and with maintenance medium, and 3) MVNs with pump flow and maintenance medium. Note that the two experiments differed not only in the presence or absence of flow reversal, but also in terms of the peak or mean pressure drop across the MVN. For MVNs with a hydraulic resistance of 1e12 Pa•s•m^{-3}, the peak pump flow rate was ~70 μL/min while the peak rocker flow rate was computed to be ~0.6 μL/min. Prior to flow, on day 7, all MVNs looked similar (Supplementary Fig. 10b). By day 16 (9 days of flow), the MVNs on the rocker with growth medium remained perfusable, but were narrow and did not appear to be aligned with the bidirectional pressure gradient (Supplementary Fig. 10b). Conversely, the MVNs on the rocker with maintenance medium regressed and lost perfusability by day 16 (Supplementary Fig. 10b). The MVNs with unidirectional flow and maintenance medium, however, were perfusable and appeared to align with the direction of flow by day 16 (Supplementary Fig. 10b) consistent with the results above. The stark difference between the perfusability and morphology of the MVNs between the rocker and pump flow using maintenance medium indicates that both the magnitude of flow and the directionality of the flow has significant effects on the long-term perfusability of MVNs.

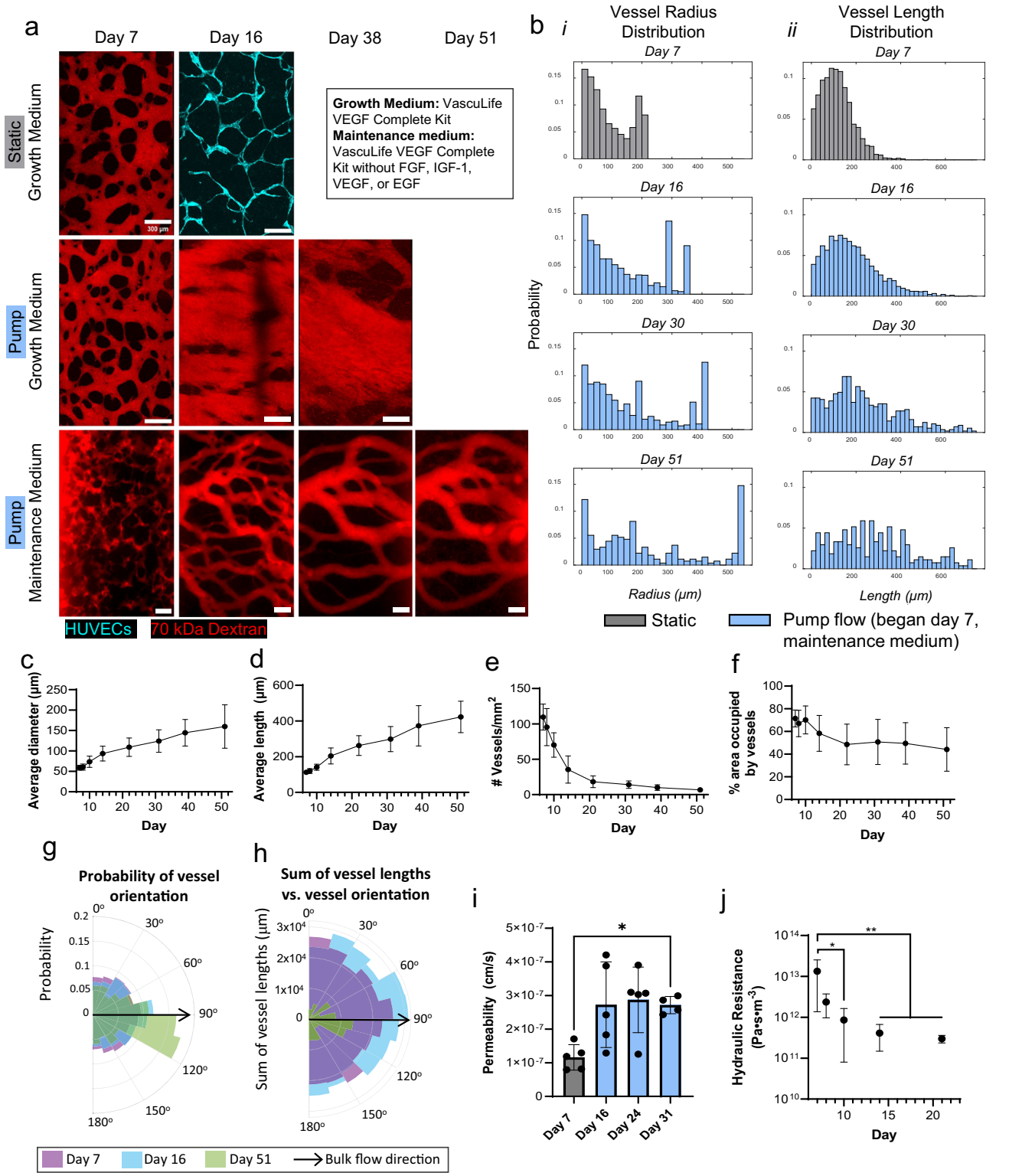

Fig. 3 | Pump flow increases the longevity of MVNs and vessels align with the direction of flow. a Representative images of MVNs grown statically, with flow and growth medium, or with flow and maintenance medium are shown perfused with dextran at selected timepoints. Scale bar is 300 µm. All the following figures are for MVNs with maintenance medium and pump flow (**b**-**j**). **b** The distribution of vessel radius (i) and length (ii) on days 7, 16, 30, and 51. The average diameter (**c**), average length (**d**), vascular density (**e**), and % area occupied by the vessels (**f**) are reported from day 7 to day 51. **g** Vessel orientation probability and **h** the orientation of the sum of vessel lengths is reported. **i** Permeability and **j** hydraulic resistance of the vessels over time. $n = 4$–11 MVNs.

Computational modeling reveals the role of flow rate, flow velocity and shear stress in the remodeling of MVNs

A previously published computational model[16] of the MVNs was adapted to analyze differences in flow characteristics between stable and regressing vessels. Analysis was performed on vessels at day 14 and vessel segments were categorized as either stable or regressing by observing whether they had regressed by day 21 (Fig. 4a). The average radius of the stable vessels (150 +/− 69 µm) was significantly higher than that of regressing vessels (40 +/

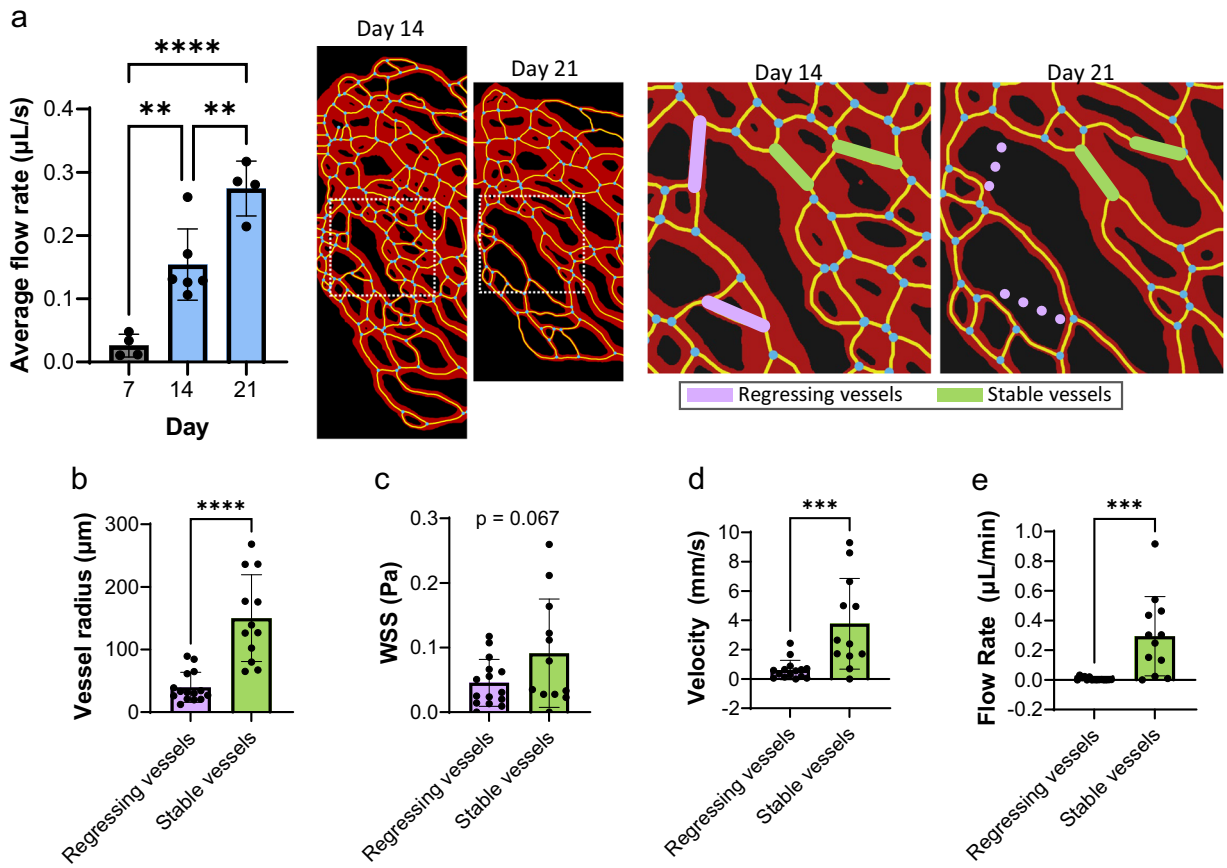

f

Regressing vessels		Velocity	Flow rate	WSS
Radius	(Pearson) r	**0.5693**	**0.8323**	0.1271
	p value	0.0267	0.0001183	0.6517
	N	15	15	15

g

Stable vessels		Velocity	Flow rate	WSS
Radius	(Pearson) r	-0.03577	**0.6253**	-0.363
	p value	0.9121	0.02968	0.2459
	N	13	13	13

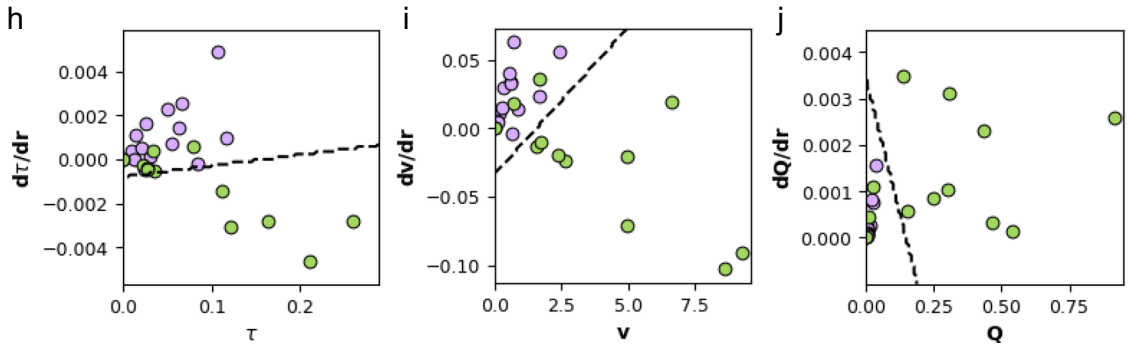

p-value	0.0488	0.0048	<0.0001
Separation accuracy	74.07%	88.89%	88.89%
Linear decision boundary equation	y = 0.005x – 0.0008	y = 0.0215x - 0.0338	y = -0.0232x + 0.0034

Fig. 4 | Stable vessels have different flow characteristics than regressing vessels. **a** Stable and regressing vessels were identified by comparing segmented images of vessels between day 14 and 21. Subsequent flow simulations and analysis were performed on the categorized day 14 vessels. The vessel radii (**b**), WSS (**c**), velocity (**d**), and flow rate (**e**) among stable and regressing vessels was compared. **f**, **g** A correlation analysis between vessel radius and velocity, flow rate, or WSS was conducted. A radius perturbation analysis was conducted and the change in WSS (**h**), velocity (**i**), or flow rate (**j**) with respect to change in radius vs. the original flow properties is reported, along with results from a 2D permutation test and linear decision boundary analysis. n = 12–15 vessel segments from 3 MVNs.

− 24 μm) (Fig. 4b). Surprisingly, however, there was no difference in the average wall shear stress (WSS, τ) in stable or regressing vessels (Fig. 4c), whereas the average flow velocity (Fig. 4d) and flow rate (Fig. 4e) were significantly higher in the stable vessels compared to regressing vessels. Since vessel radius plays a significant role in the level of flow a vessel receives, the correlation between vessel radius and the various flow parameters was analyzed (Fig. 4f, g). In the regressing vessels, there was a strong and significant correlation between vessel radius and velocity (r = 0.5693), and radius and flow rate (r = 0.8323) (Fig. 4f). In the stable vessels, there was a significant and strong correlation (r = 0.6253) between the vessel radius and flow rate (Fig. 4g). Note, the vessel diameters were measured from 2D maximum image projections in the x-y plane, which do not consider the roughly two-to-one ellipticity ratio of the vessel cross sections (Supplementary Fig. 11). While WSS is influenced by the velocity gradient at the vessel wall, it also depends on vessel diameter. Here, regressing vessels exhibited reduced diameters, which led to higher flow velocities and rates for a given volumetric flow. However, because WSS is proportional to both the velocity gradient and the dynamic viscosity, the increased velocity in narrower vessels was offset by the smaller diameter, resulting in similar WSS values between regressing and stable vessels. Thus, even though flow velocity and rate increased, the concurrent decrease in vessel diameter maintained the WSS at comparable levels across these groups. The computational model was then used to systematically perturb the vessel diameters individually, decreasing their diameter by 10% and observing changes in WSS, velocity (v), and volume flow rate (Q) (Fig. 4h–j). Most regressing vessels experienced a decrease in their WSS (Fig. 4h) and velocity (Fig. 4i), while most stable vessels experienced an increase in WSS (Fig. 4h) and velocity (Fig. 4i). All vessels experienced a decrease in flow rate because of the perturbation (Fig. 4j). The vessels were next compared in a 2D parameter space: one dimension was the change in flow parameter (ie. τ, v, Q) with respect to the change in radius, and the second dimension was the absolute value of the flow rate. A 2D permutation test showed that the regressed vessels were significantly different than the stable vessels for all three flow parameter space comparisons (Fig. 4h–j). The separation accuracies of a linear decision boundary analysis were about 74% for the τ space and about 89% for the v and Q spaces (Fig. 4h–j). Computational modeling thus revealed that velocity and flow rate play a critical role in the remodeling process of the MVNs, somewhat more so than shear stress in the present experiments.

Continuous perfusion reduces vessel inflammation

The concentration of inflammatory cytokines produced by static MVNs and MVNs cultured with flow (both with maintenance medium) was analyzed in a multiplexed inflammatory cytokine assay and compared for early time points (day 9 and day 11) before static MVNs significantly regressed and lost perfusion (Fig. 5a). By day 9, the concentrations of GM-CSF (Fig. 5b) and IL-1RA (Fig. 5d) were significantly lower in flow MVNs compared to static MVNs while there was no difference in IL-1β (Fig. 5c) and the concentration of IL-8 (Fig. 5f) was lower in flow MVNs by day 11. IL-6 (Fig. 5e) was significantly increased in flow MVNs on day 9 but dropped to comparable levels to static MVNs by day 11. These results indicate that inflammatory cytokines significantly decrease within the first few days of adding pump flow to MVNs. Long-term tracking of inflammatory cytokines was also conducted. The supernatant from MVNs at days 7 (static), 14 (one week of flow), and 22 (two weeks of flow) was collected after 24 hours of conditioning with the MVNs (Fig. 5g). The concentration of GM-CSF (Fig. 5h), IL-1β (Fig. 5i), and IL-8 (Fig. 5l) significantly decreased with 2 weeks of flow, indicating the MVNs became less inflamed and consistent with the shorter-term experimental results. These cytokines are known to have various functions in the immune response: GM-CSF has been shown to act on macrophages and neutrophils by increasing their survival and activation[17], IL-1β is known to induce expression of VCAM-1, which in turn contributes to leukocyte recruitment[18], and IL-8 primarily acts to recruit monocytes and macrophages to an inflamed site[19]. GM-CSF, IL-1B, and IL-8 may be secreted from both ECs and fibroblasts (FBs)[17,19,20]. While the other analyzed cytokines are known to play a role in vascular inflammation and remodeling, their concentrations did not decrease significantly with flow and time (Fig. 5j, k, Supplementary Fig. 12). While the concentration of IL-6 tended to decrease over time, the differences did not reach statistical significance. This may be due to its role in chronic inflammation and tissue repair, whereas IL-8 is primarily associated with acute inflammation[21]. Furthermore, on day 7, growth medium and static conditions were used, while on days 14 and 22 maintenance medium and flow conditions were used, therefore the changes in cytokine concentrations were attributed to both the change in medium and the introduction of flow. To study the role of media type on the concentration of inflammatory cytokines, static 2D transwell cultures with ECs and FBs were conducted up to day 22 (Supplementary Fig. 13). While the concentrations of GM-CSF and IL-8 significantly increased in growth medium compared to maintenance medium at later time points, there were no differences in the concentrations of IL-1β, IL-1RA, or IL-6 between the two media types at days 14 and 22 (Supplementary Fig. 13). These data indicate that media type significantly impacts the inflammatory state of ECs. Importantly, the reduction in IL-1β and IL-1RA observed in both short- and long-term flow-conditioned MVNs is likely attributable to continuous perfusion rather than media type. These findings underscore the highly inflamed state of vascular networks lacking flow and/or with high levels of growth factors and argue for the use of continuous flow and maintenance medium for experiments in which the inflammatory state of the vasculature is key.

Bulk RNA sequencing provides an assessment of MVN response to flow

To identify differentially expressed genes (DEGs) as a function of duration of flow conditioning, the transcriptomes of the ECs and FBs from MVNs at days 7, 15 (8 days of flow), and 24 (17 days of flow) were analyzed using bulk RNA sequencing (RNAseq) (Fig. 6a). The pairwise comparisons demonstrated distinct clustering patterns (Fig. 6b, c). Volcano plots for the pairwise comparisons show the up-regulated and down-regulated (red) DEGs (p.adjust < 0.05, $|\log_2$ fold change$|>1$) (Fig. 6d). *ICAM-1* was downregulated in ECs at day 24 compared to days 15 and 7, and *VCAM-1* was downregulated in ECs at day 15 compared to day 7, potentially indicating a less inflamed state. Inflammation triggers increased expression of ICAM-1 and VCAM-1, which facilitate leukocyte transendothelial migration[22–24]. *VCAM-1* gene expression has been shown to be inhibited in regions of laminar flow, mediated through shear stress-regulated genes such as endothelial nitric oxide synthase or superoxide dismutase[18]. mRNA expression of *HMOX1*, *GCLM*, and *NQO1* was upregulated in ECs at day 15 and day 24. HMOX1, GCLM, and NQO1 proteins have been shown to be upregulated in ECs exposed to atheroprotective shear flow[25,26]. Furthermore, several key EC junctional genes were downregulated (Supplementary Table 1). However, functional assays demonstrated that endothelial barrier integrity remains stable, as confirmed by permeability measurements (Fig. 3i) and VE-cadherin protein localization (Supplementary Fig. 8), which showed no appreciable loss at the cell junctions. This suggests that post-transcriptional mechanisms and protein stability help maintain critical junctional complexes despite reduced mRNA expression. Live/dead staining at days 7 and 14 confirmed high cell viability at both timepoints (Supplementary Fig. 9), further supporting our conclusion that chronic flow conditions do not induce cytotoxicity or apoptosis in HUVECs. The total number of DEGs is reported (Fig. 6e). The day 24 vs. day 7 pairwise comparisons yielded the highest number of DEGs in both the ECs and the FBs. Venn diagrams show the grouped overlap of up- and down-regulated DEGs among the three pairwise comparisons for ECs and FBs (Fig. 6f). Interestingly, there were no DEGs only common between the day 24 vs. day 15 and day 15 vs. day 7 pairwise comparisons for the ECs or the FBs, indicating continuous transcriptomic changes in both cell types. 8 DEGs were common to all three EC pairwise comparisons, and 13 DEGs were common to all FB pairwise comparisons. *ITGB5*, common among all EC pairwise comparisons, encodes integrin subunit beta 5, has been shown to play a role in lung endothelial survival and migration[27]. *SRXN1* was common among all EC and FB pairwise comparisons and its encoded protein has been shown to

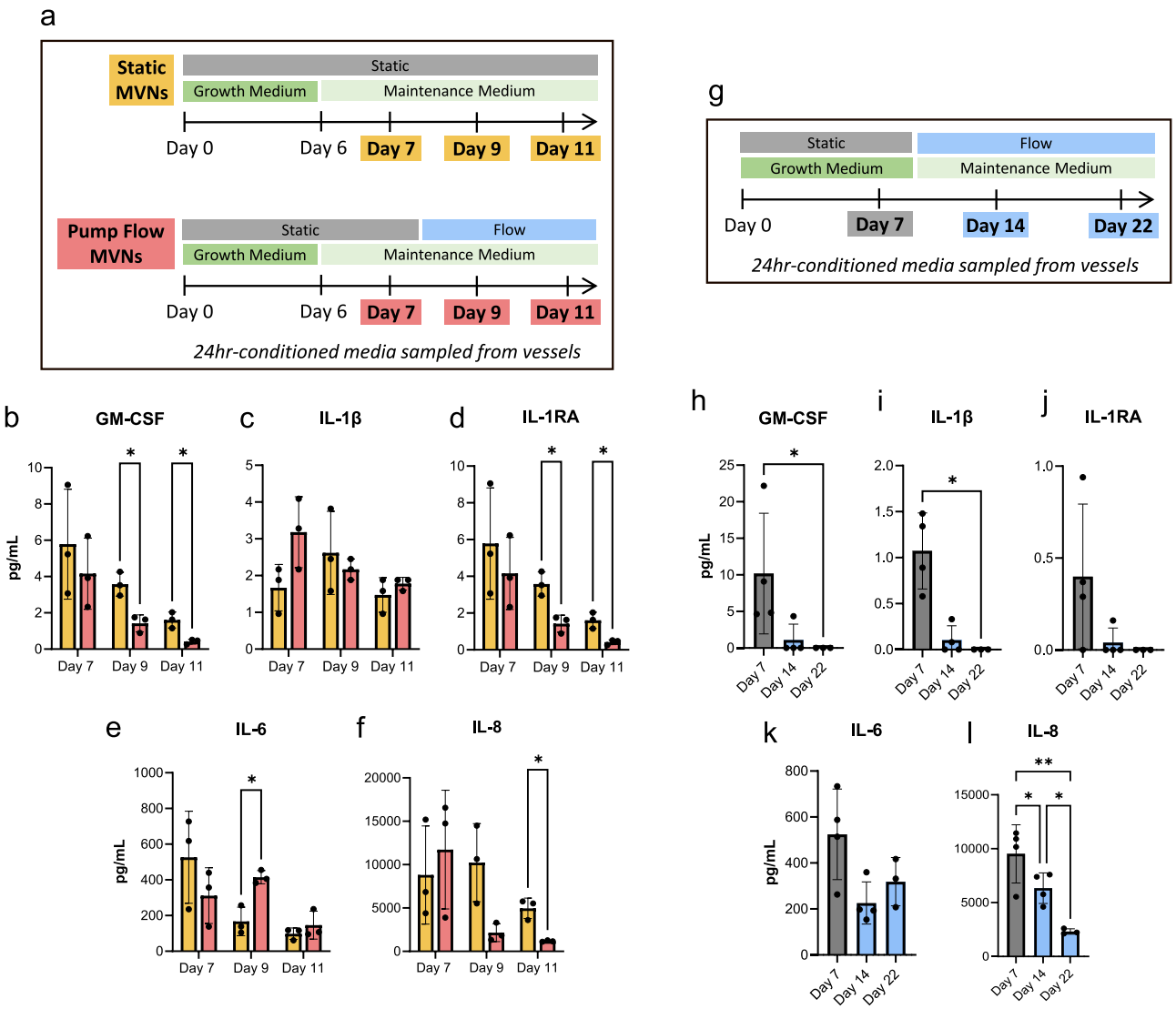

Fig. 5 | Flow reduces the magnitude of the concentration of selected inflammatory cytokines. a, **g** Experimental timeline indicating the supernatant sampling timepoints. **b**–**f**, **h**–**l** Concentration of inflammatory cytokines across timepoints. The selected cytokines were (**b**, **h**) GM-CSF, (**c**, **i**) IL-1β, (**d**, **j**) IL-1RA, (**e**, **k**) IL-6, (**f**, **l**) IL-8. $n = 3$–4 MVNs.

protect neurons[28] and cardiac progenitor cells[29] from oxidative stress injury. GO pathway analysis (Fig. 6g) revealed differential expression of hypoxic pathways in both the ECs and FBs, which may point to the differential expression of *SRXN1* in the ECs and FBs. *EPHX1*, which has been shown to have detoxification properties[30], was also upregulated in all pairwise comparisons. Among the FB pairwise comparisons, *GPX3* and *ADM* were common DEGs of interest. *GPX3* is known to be upregulated in oxidative stress conditions and protects epithelial cells from oxidative damage[31]. Adrenomedullin, the protein encoded by *ADM*, has been shown to induce vasodilation[32], which is in line with the MVN morphological changes presented here. The GO pathway analysis further revealed that by two weeks of flow conditioning (day 24 pairwise comparisons), the ECs were involved in pathways related to cell adhesion, lung development and ECM organization, specifically collagen fibril organization (Fig. 6g, Supplementary Fig. 14). The ECs also expressed the pathways of negative regulation of cell death and negative regulation of apoptotic process, indicating endothelial survival (Supplementary Fig. 14). Several collagen genes were upregulated by the ECs, namely *COL1A1*, *COL1A2*, and *COL12A1*. The corresponding proteins, as well as several other collagens, were upregulated as shown by proteomics analysis through mass spectrometry in a static MVN system within 14 days of culture since seeding (Supplementary Figs. 15, 16). Furthermore, 33% of the matrix was newly deposited by the cells in this same 14-day period (Supplementary Fig. 16). Interestingly, the large changes in matrix synthesis were not observed when the endothelial cells or fibroblasts were individually cultured under the same conditions, suggesting that bi-directional signaling between the two cell types is critical for these changes to occur (Supplementary Fig. 15). A similar trend would be expected for the flow system presented in the present study as the same two cell types were used. Other matrix proteins that were clearly present in the static experiments, however, notably fibronectin (FN1) and heparin sulfate (HSPG2), were only slightly up- or down-regulated, respectively, under flow conditions. The FBs were also involved in extracellular matrix reorganization, collagen fibril organization, and blood vessel development (Fig. 6g). By two weeks of flow conditioning, several hypoxia-related pathways were differentially expressed in the FBs, indicating a possible lack of oxygen (Fig. 6g). Perivascular FBs in a zebrafish mode have been shown to help regulate blood vessel diameter through the secretion of collagens[33]. The "collagen fibril organization" GO pathway was differentially expressed and several collagen-related genes were significantly upregulated in the FBs at d24vsd7, including *COL11A1*, *COL27A1*, *COL5A2*, and *COL14A1*, which may indicate increased collagen production by the FBs. Furthermore, several pathways related to biosynthetic and metabolic process were differentially

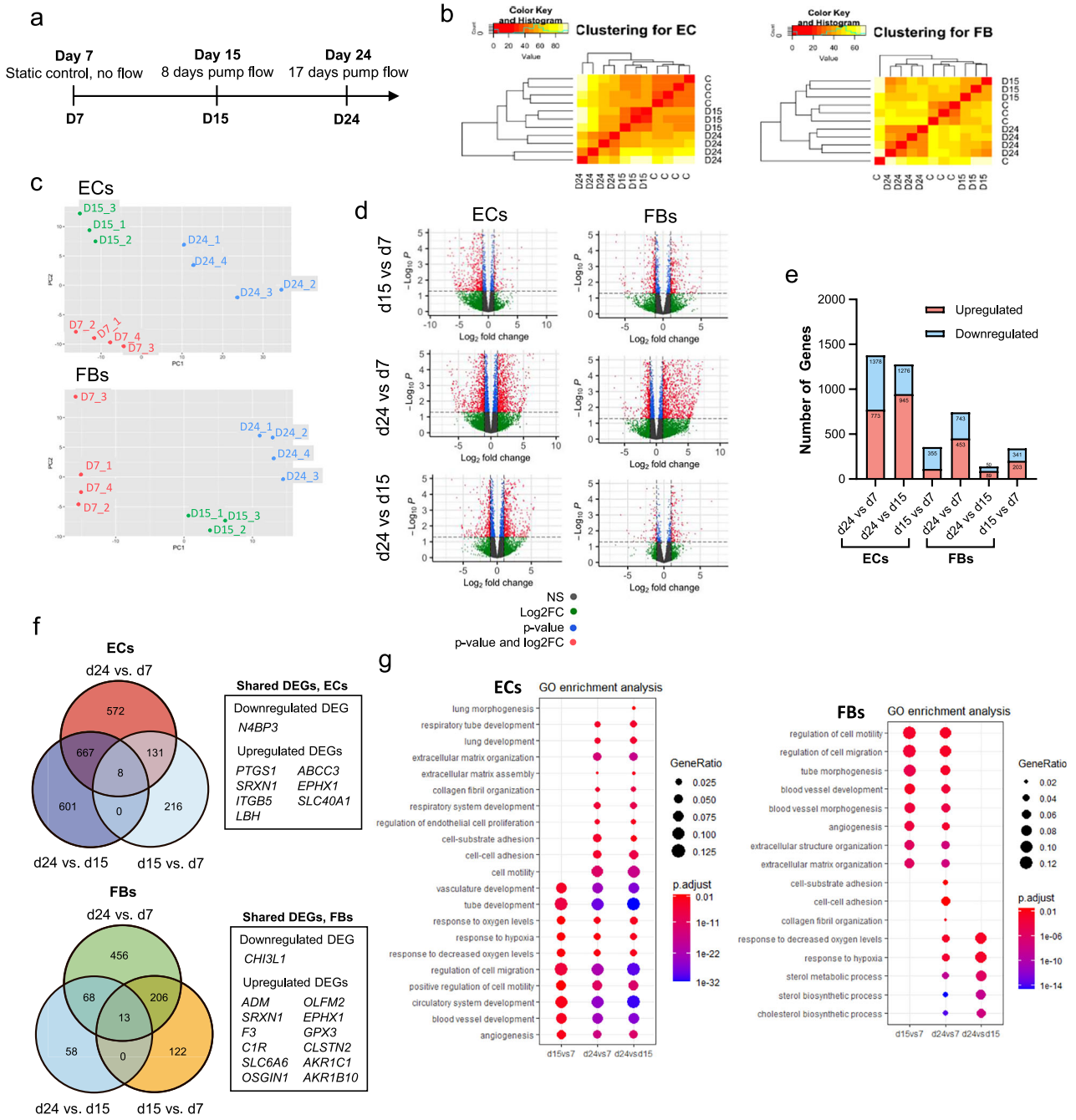

Fig. 6 | Bulk RNAseq of the ECs and FBs revealed differential pathway expression between days 7, 15 (8 days pump flow), and 24 (17 days pump flow). a Cells were isolated and prepared for RNA extraction on days 7, 15, and 24. Heatmaps (**b**) and PCA plots (**c**) showing clustering of the ECs and FBs for each pairwise comparison. **d** Volcano plots for genes in the ECs and FBs for each pairwise comparison with annotated DEGs of interest. **e** Number of DEGs up- and down-regulated in the ECs and FBs. **f** Venn diagrams showing the overlap of DEGs among the pairwise comparisons. Inset table lists the DEGs common to all three pairwise comparisons for the ECs and FBs. **g** GO pathway analysis comparing the ECs and FBs across the pairwise comparisons timepoints. $n = 3–4$ samples, each sample with 3–4 pooled MVNs.

expressed in the FBs at d24vsd7, which may further indicate excessive collagen production by the FBs. FB production of collagen is known to be energy intensive and requires unique biosynthetic demands of the FBs[34]. The RNAseq results provide insights into the dynamics of the EC and FB phenotypes over long term MVN perfusion.

Discussion

The purpose of this work was to investigate the effects of continuous recirculating flow on the morphology, function, cytokine profile and transcriptome of MVNs grown in microfluidic devices. These systems have been extensively used for studies of primary and metastatic cancer[35] and for various organ-on-chip models[36]. However, the vascular networks have a limited lifetime, and the useful period of experimentation is typically several days after the MVN forms. But in many applications, such as studies of metastatic outgrowth or organ maturation and function, longer-term studies are required, and in studies of inflammation and immune cell recruitment, the concentration of cytokines by the vasculature is critical. In the present study, flow is used to recover the perfusability of regressing MVNs, which subsequently maintain perfusion for at least 51 days with continuous flow (Fig. 7). This enabled us to observe how MVNs exposed to physiological flow remodel through a combination of vessel dilation and regression and how their phenotype and state of inflammation change

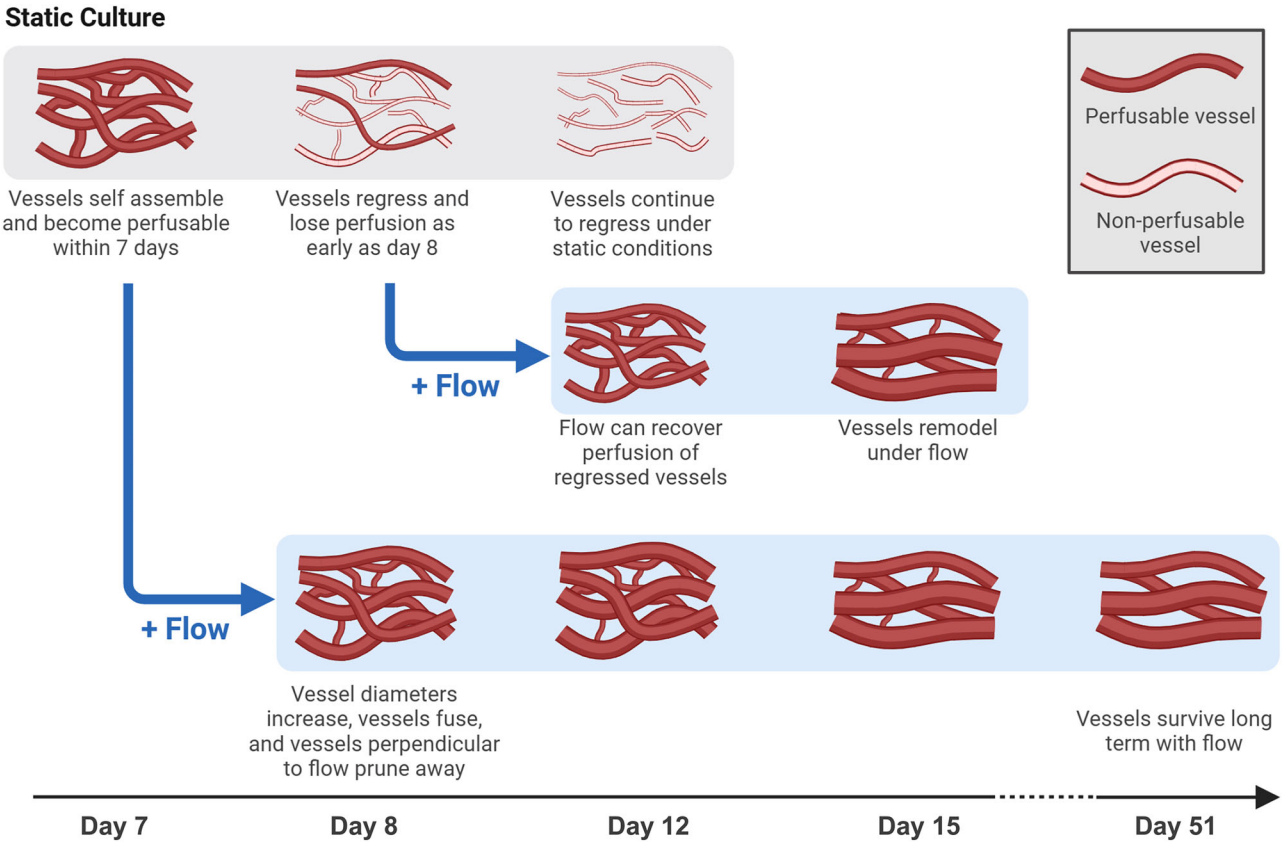

Fig. 7 | Summary of the effects of flow on the remodeling of MVNs. Under static culture, MVNs lose perfusion, regress, and die. Adding flow to regressing vessels rescues perfusion and vessels remodel in response to flow. Adding flow to initially healthy and perfusable vessels results in vascular remodeling and long-term perfusion (for at least 51 days).

under flow compared to standard, static conditions. It also provided new insights into the extent to which these networks can be stabilized and how flow and media composition can drive changes in both network stability and the local inflammatory state.

Over the course of 44 days of flow, regression of vessels perpendicular to the pressure gradient was observed, consistent with previous findings[37], whereas the diameters of vessels parallel to the pressure gradient increased over time. The permeability of the MVNs remained low, although contrary to some previous studies, continuous flow caused an increase rather than a decrease in permeability, despite a reduction in inflammatory cytokines. A previous study using a similar MPS reported similar permeability values for MVNs under hydrostatic pressure-driven flow[10]. The higher permeability on Day 31 may have been a result of a lower effective dextran concentration[38,39] because of the method used to introduce dextran when the pump was connected to the device.

While significant remodeling was anticipated, it was also expected that the networks would eventually stabilize based on a long history of observations in vivo. This expectation is the basis for what has come to be known as the set point theory[40], wherein vessels experiencing higher than physiological WSS tend to increase in diameter until the WSS attains a certain value. Conversely, vessels with a WSS less than the set-point value constrict. This is but one of many biological consequences of endothelial shear stress, which has been studied extensively both in vivo and in vitro in the context of arterial disease (see ref. 12 for a comprehensive review). For example, in response to an arteriovenous shunt in canine observed 6–8 months postoperatively, the radius of the shunt vessel increased with increased flow load until the wall shear rate reached the control, pre-shunt value[41]. This may suggest that longer culture time is required for the MVNs to reach stability. Furthermore, it has been shown in a zebrafish model that peak WSS imposed by individual red blood cells through capillaries can provide sufficient mechanical stimulus for microvascular vessels to reach their stable radius[42]. The MVNs in this study, however, did not approach an average set point and our results failed to provide support for the set point theory. Instead, vessel fate seemed more strongly linked to the flow rate passing through the vessel, with those vessels conveying a lower flow rate tending to regress.

There are several possible explanations why the average diameters of the MVNs continued to increase. The continued expansion of vessel diameters observed may have been due to the presence of a high concentration of growth factors in the medium as the progressive dilation was significantly reduced when using maintenance medium. When the growth factors were removed, major vessel segments tended to stabilize maintaining a nearly constant diameter between days 16 and 51 and vascular network resistance remained nearly constant on days 14 and 22. Changes in stiffness and composition of the surrounding gel may also have contributed to the changing vascular morphology[43]. In a static 3D in vitro platform similar to the one presented in this study, the elastic modulus of the hydrogel with embedded ECs and FBs increased ~13-fold in the first seven days of juxtacrine co-culture and thereafter maintained a somewhat constant elastic modulus through day 14[4]. The lack of pericytes and smooth muscle cells may also contribute to the continued increase in diameter. Pericytes are known to regulate vascular diameter and vascular blood flow in the capillary bed through vasoconstriction and vasodilation[44], and smooth muscle cells are known to play a role in vasoconstriction and vasorelaxation in the arterioles[45]. The heterogeneity of the MVNs may have contributed to the continuous vascular remodeling, whereby the initial morphology and structure of the MVNs at day 7 was not the optimal organization for continuous flow perfusion. The transcriptomic data suggest yet another explanation. Between days 7 and 24, there is a strong indication that the fibroblasts are hypoxic, even under continuous flow. If so, the physiological

response would be to signal an increase in perfusion, which would correspond to an increase in vessel diameter. Clearly, vasodilation and constriction are multifaceted, dynamic processes, that depend on many factors in addition to WSS.

MVNs perfused with flow with alternating direction, conversely, did not show increases in vessel diameter over time. Despite the extensive literature on the effects of pulsatile or flow with alternated direction on endothelial function in the context of arterial disease, relatively little research has addressed these effects in the microcirculation. This is likely due, at least in part, to the fact that flow with alternated direction is uncommon in the small vessels under normal physiological conditions since flow in the capillaries is generally thought to be unidirectional and, while pulsatile, the temporal fluctuations are small relative to those in the larger arteries. Despite this, rocker platforms are increasingly used in MVN experiments, and the effect of flow with alternating direction on MVNs needs to be characterized. The observed deterioration of the MVNs under rocker flow compared to continuous flow suggests that either the directionality of the flow is significant or that some minimum flow rate must exist for MVNs to maintain perfusability. Due to physical constraints, the magnitude of the pressure gradients generated by the rocker was typically lower than that in unidirectional flow (~3.9×10^5 Pa/m for the pump and ~3.3×10^4 Pa/m for the rocker) and this could have contributed to the differences observed. This is further supported by the computational simulations conducted on stable and regressing vessels, which showed that stable vessels had significantly higher flow rates than regressing vessels. As for biophysical mechanisms, one potential mechano-sensor would be the primary cilium present in most mammalian cells[46] including endothelial cells. This singular structure is known to elicit a variety of cellular signals, has been shown to be responsible for preventing vessel regression, and could be capable of sensing the direction of flow[47]. This comparison highlights the significance of the magnitude and directionality of flow on the dynamics of MVNs.

Computational modeling of flow through MVNs revealed several interesting findings. One study thus far has demonstrated long term perfusion for up to 50 days and showed that vessels located in regions of low flow were more likely to regress, but did not characterize the function or phenotypes of the vasculature[37]. In addition to the apparently predominant role of flow rate in determining the stability of a vessel, the tendency for regressing vessels to experience a decrease in their WSS when their diameters are reduced by 10% may indicate that their morphology and location relative to other vessels may also influence their stability. The application of either a constant flow rate or constant pressure drop across the MVNs may also influence their stability; e.g., an increase in vessel diameter under a constant flow rate decreases WSS, while under a constant pressure gradient the WSS increases[42]. However, the microfluidic pump used in this study provides neither a constant pressure nor a constant flow rate.

In addition to influencing MVN morphology, flow also played a role in lowering inflammation of the MVNs. Several key cytokine concentrations rapidly decrease within 2–4 days in flow conditioned MVNs compared to static MVNs. The increase in IL-6 in flow MVNs at day 9 may indicate that IL-6 plays a transient role in the remodeling of the MVNs in response to flow. The results from the short-term static and flow MVN comparison are consistent with the long-term inflammatory cytokine data and indicate that flow alone rapidly induces a reduction in several inflammatory cytokines compared to static MVNs. The cytokine concentrations on day 7 were sampled from MVNs before exposure to flow, which indicates that the initial state of the system is relatively inflamed. Initially higher concentrations of cytokines at day 7 may be a result of the use of a fibrin and thrombin-based hydrogel used in cell seeding. Fibrin is known to be involved in inflammation and cytokine/chemokine production as IL-6 and MCP-1 were shown to accumulate in a fibrinogen-dependent manner in mice[48]. Thrombin is known to promote activation and inflammation of the brain endothelium[49]. Data obtained in static conditions show that there is significant remodeling of the ECM over 14 days, which may decrease the presence of fibrinogen as other matrix proteins are added to the matrix and thus reduce inflammatory effects. The concentration of several inflammatory cytokines subsequently decreased with 7 and 15 days of flow in maintenance medium, indicative of a gradual transition to a healthy, less inflamed state. This has several important consequences for the application of in vitro MVNs to model disease processes. The general reduction in inflammatory cytokines is consistent with an atheroprotective flow, which is characterized by high unidirectional laminar shear stress[50]. Additionally, the significant reduction of IL-8 over time is also consistent with a less inflamed state as IL-8 has been shown to enable adhesion of monocytes[51] and activation of neutrophils[52]. In a study using a static co-culture of HUVECs and normal human lung FBs in a fibrin gel in a microfluidic chip, the concentration of secreted IL-6 decreased from day 3 to 5, but there were no changes in IL-8 or MCP-1[53], which may indicate that flow or longer culture time is required for secreted IL-8 to decrease. The reduction in IL-8, IL-1β, and GM-CSF also suggests a shift towards a less angiogenic state, consistent with our gene expression analysis. IL-8 is increased in the early stages of angiogenesis[54], and GM-CSF[55] and IL-1β[56] promote angiogenesis. This result is further supported by our findings showing a reduction in the gene expression in the ECs of *ICAM-1* between day 24 and days 15 and 7, and *VCAM-1* between days 15 and 7. IL-1β is known to induce VCAM-1 expression[18], therefore a reduction in IL-1β may contribute to the lower expression of *VCAM-1* seen here. Furthermore, MMP-2 has been shown to degrade IL-1β[57], thus the reduction in IL-1β in this system may be attributed to the increase in *MMP-2* mRNA expression in the FBs at day 24. High, sustained levels of MCP-1 are consistent with increased mRNA expression in the FBs at day 15 and day 24 compared to day 7 control. Overall, we observed that continuous perfusion induces significant remodeling of MVNs, characterized by transcriptional shifts, reduced inflammatory signaling, and preserved barrier function. While our data strongly support a flow-driven adaptive response, we acknowledge that additional factors, including cellular age, the onset of senescence, and ECM maturation, may also contribute to the observed phenotypic changes.

Transcriptomic analysis further revealed pointed towards the types and drivers of the vascular remodeling. Lung morphogenesis related pathways were differentially expressed and HUVECs are known to be plastic, which may indicate the HUVECs were adopting a lung-like phenotype in response to the long-term co-culture with the lung FBs[58]. Several ECM-related pathways were also differentially expressed, indicating that both the HUVECs and FBs were involved in matrix remodeling throughout the two weeks of flow conditioning. The ECs had several highly upregulated collagen-related genes, *COL1A1*, *COL1A2*, and *COL12A1*, which correspond to proteomics data from the remodeling ECM of static MVNs, likely driving the deposition of collagen during the flow-induced vascular and ECM remodeling. Hypoxia-related pathways are differentially expressed in the ECs and the FBs. The ECs may be expressing hypoxic pathways because of the flow rate-mediated vascular remodeling, where the population of ECs lining regressing vessels that are receiving inadequate levels of flow rate may be hypoxic. The FBs may be expressing hypoxic pathways due to proliferation over time combined with the reduction in vascular density from 35 vessels/mm^2 at day 14 to 18 vessels/mm^2 at day 22 (Fig. 3e), which may be below some threshold for adequate oxygen supply. The ECM of flow conditioned MVNs has lower diffusivity to 70 kDa Dextran compared to static MVNs, which may point to a reduction in oxygen diffusivity[9]. Cells in organs and tissues are typically within 200 μm from a blood vessel to have adequate nutrient and oxygen supply[59]. Further studies are required to identify methods to ensure the cells in the ECM are receiving adequate amounts of oxygen. Overall, our data demonstrate that chronic perfusion induces an adaptive endothelial response rather than dysfunction. Although several key junctional genes are downregulated at the mRNA level, barrier integrity and VE-cadherin protein localization remain stable, indicating post-transcriptional compensation. High cell viability further supports a shift toward a quiescent phenotype under flow. GO term analysis reveals upregulation of pathways related to cell-matrix adhesion, cytoskeletal organization, proliferation, angiogenesis, and survival, suggesting active

remodeling and enhanced regenerative capacity. Together, these findings indicate that sustained flow promotes physiological endothelial plasticity, maintaining vascular function and readiness for remodeling.

While this study provides valuable insights, the following limitations should be considered. The computational model has several inherent assumptions that may result in errors of the absolute flow estimates made here. First, the model assumes steady, laminar flow. The average Reynolds number (Re) calculated was found to be 2.6 and the maximum Re was 11.6, validating the assumption of laminar flow, but suggesting that some small effects of inertia could be present. More importantly, errors in the measurement of vessel diameters have a particularly strong effect on the estimated hydraulic resistance of the vessel segments owing to the inverse fourth power dependence of vessel flow resistance (R) on radius (r); $R = 8\mu L/\pi r^4$. For example, vessel diameters were measured from 2D maximum image projections, in the x-y plane, which do not consider the roughly two-to-one ellipticity ratio of the vessel cross sections, the high degree of variability in the cross-sectional diameters along the segment length, or the effects of flow in the z-direction. For the transcriptomics, flow sensitive genes such as KLF-2 did not show differential gene expression in the flow MVNs compared to day 7 static controls. The half-life of KLF2 mRNA was previously reported to be 56 min[60], significantly shorter than the several hours-long time required to digest, extract, and sort the cells from the microfluidic devices. Furthermore, the mRNA from the ECs was extracted after a relatively long flow exposure time, whereas in the literature ECs are typically exposed to shear flow for 16–72 h[61–63].

This MPS extends upon existing models by enabling the capability to study hemodynamically modulated processes, such as vascular regression/reperfusion, drug distribution, or metastatic dissemination. Subsequent investigations might extend this research by incorporating organ-specific cells or patient-derived cells to study the role of hemodynamics in organ- and patient-specific diseases.

In conclusion, we use a low dead volume microfluidic pump that is easy to fabricate and assemble to provide long-term, continuous recirculating flow through MVNs. This MPS extends existing models by enabling the capability to study hemodynamically modulated processes, such as vascular regression/reperfusion, drug distribution, or metastatic dissemination. We show that continuous perfusion of a microvascular microfluidic system is capable of long-term (at least 51 days) perfusion. During perfusion, the MVNs remodel: thin vessels prune and vessels that align with the direction of flow predominate, and their diameter increases. The addition of flow to regressed MVNs is observed to recover perfusability to initially non-perfusable networks. Computational modeling suggests flow rate is a determining factor in the regression or stability of individual vessel segments. Static MVNs tend to be in an inflamed state, but the inflammation is reduced with continuous perfusion. This, in combination with previous findings that co-culture of endothelial cells and fibroblasts produced a dramatic change in tissue stiffness and matrix composition, is further evidence of an ongoing remodeling process. Finally, transcriptomic analysis shows that extracellular matrix reorganization, hypoxia, and vascular development are all enhanced in the presence of flow. Subsequent investigations might extend this research by incorporating organ-specific cells or patient-derived cells to study the role of hemodynamics in organ- and patient-specific diseases. These findings pave the way to developing long-term MPS and models to study complex hemodynamic processes such as drug distribution.

Methods

Cell culture

Immortalized human umbilical vein endothelial cells (ECs) (Lonza, CC: 2935, immortalized and transfected to express blue fluorescent protein as previously described[64]), and human primary normal lung fibroblasts (FBs) (Lifeline, FC-0049) were used in this study. ECs were cultured with vascular growth medium using the vendor's protocol (VascuLife VEGF Endothelium Medium Complete Kit, Lifeline) and used at passage 8; FBs were cultured with fibroblast medium following vendor's protocol (FibroLife S2 Fibroblast Medium Complete Kit, Lifeline) and used at passage 5. For transwell experiments, 20,000 ECs were seeded onto the transwell inserts of a 24-well transwell plate with 3 μm pore polycarbonate membrane (Sigma), and 2000 FBs were seeded in the well plate.

Microvascular network formation

ECs and FBs were detached using Accutase (Sigma, SCR005), pelleted, and resuspended in vascular growth medium supplemented with 4 U mL^{-1} thrombin (Sigma, T4648-1KU) at concentrations of 26 $\times 10^6$ mL^{-1} and 6 $\times 10^6$ mL^{-1}, respectively. Equal volumes of resuspended HUVECs and FBs were mixed, then combined with an equal volume of fibrinogen (6 mg mL^{-1}, Sigma 341578) in phosphate buffered solution (PBS, Gibco 10010031), and injected into the gel ports of the microfluidic devices. The devices were placed in a humidified incubator for 12 min to allow the hydrogel to polymerize, and then vascular growth medium was added into the device medium channels. Medium in these channels was changed daily and MVNs became perfusable by day 7.

Fabrication of microfluidic device and pump

The design of the microfluidic device and pump were created using Autodesk Fusion 360. The device was composed of a central gel channel flanked by two media channels. The gel channel was 3 mm wide, 7 mm long, and 0.5 mm tall, and the media channels were 3 mm wide and 0.5 mm tall. The pump design was used as described previously[13]. The device and pump molds were milled using a Bantam Tools Desktop CNC Milling Machine (Bantam Tools). Polydimethylsiloxane (PDMS, Dow Corning Sylgard 184, Ellsworth Adhesives) was mixed at a 10:1 elastomer to curing mass ratio, degassed for 40 min, poured into the device and pump molds, degassed a second time for 25 min, then placed and cured at 65 °C overnight. Individual devices and pumps were cut out, and the ports of the gel channel, media channel, and pump were punched using biopsy punches (Integra Miltex). The silicone membrane (LMS, Amazon) was cut to size and ports were punched using biopsy punches (Integra Miltex). The devices, pumps, and silicone membranes were sterilized in an autoclave for 25 min. The devices and #1 glass cover slips (VWR) were exposed to plasma (Harrick Plasma), bonded together, and placed in an 75 °C oven overnight. The pumps were similarly bonded through plasma exposure in a two-step method: first the bottom half of the pump was bonded to the silicone membrane, and then the bottom half and silicone membrane group was bonded to the top half of the pump, and placed in a 75 °C over overnight, as previously described[13].

Application of flow to MVNs

The pump was connected to the device using silicone tubing (Miniature Firm EVA Tubing for Air and Water, 1883T3, McMaster Carr) on either day 7 (long-term experiments) or day 12 (perfusion recovery experiments). All flow experiments used a pump input pressure of 6 kPa. Long-term flow experiments were performed with maintenance medium after day 7 (VascuLife VEGF Endothelial Medium Complete Kit without rh VEGF LifeFactor, rh FGF basic LifeFactor, rh IGF-1 LifeFactor, and rh EGF LifeFactor, Lifeline), and perfusion recovery experiments were performed with growth medium (VascuLife VEGF Endothelium Medium Complete Kit, Lifeline) after day 12. During pump operation, the two device reservoirs opposite the pump were blocked to create a closed fluidic system. Media in pump devices was changed every two days.

The corresponding flow rate through and pressure drop across the MVNs was dependent on the hydraulic resistance of the MVNs and followed relationships according to Supplementary Fig. 1. This input pressure was chosen based on computational simulations that predicted physiological average wall shear stresses of 1 Pa, as previously described[11,13]. The steady state flow rate depended both on the pressure difference across the pump capacitors and the hydraulic resistance of the MVNs and channels connected to the pump. The steady state flow rate for different pressure

inputs and characteristic hydraulic resistances was measured (Supplementary Fig. 1). The hydraulic resistance was measured using a previously discussed protocol[11]. The corresponding pressure drop was calculated using

$$\Delta P = QR \tag{1}$$

where ΔP is the pressure drop, Q is the steady state flow rate and R is the hydraulic resistance of the connected channels. The pump flow rate increased linearly with input pressure (Supplementary Fig 1).

A custom-built rocker was used to generate hydrostatic pressure-driven flow. 5 mL syringes were inserted into the microfluidic device ports. The syringes were all filled equally to achieve a height of 20 mm. The devices with syringes were then placed inside of a box with a dish containing PBS and placed on the rocker platform. The rocker tilted 43° such that one media channel was elevated higher than the second media channel, producing a hydrostatic pressure difference to drive flow through the MVNs (Supplementary Fig. 7). This tilt was maintained for 10 min, after which point the rocker tilted 86° in the opposite direction to reverse the hydrostatic pressure difference and continued tilting or "rocking" every 10 min. Every 48 h, the medium in the syringes was replaced with fresh medium. This setup produced a maximum hydrostatic pressure difference of 98 Pa, which dissipated to 96 Pa during the 10 min for MVNs with 1e13 Pa-s/m^3 hydraulic resistance. This translates to an initial bulk flow rate of 0.59 μL/min and dissipated to 0.58 μL/min after 10 min. The hydrostatic pressure difference created by the rocker can be estimated following a similar analysis shown in Supplementary Fig. 17, and, using the hydraulic resistance of the MVNs, the flow rate can be calculated as specified above.

The microfluidic pump features a low dead volume (230 μL), recirculating flow, and flow rates ranging from 8 to 240 μL min^{-1}, allowing for continuous, long-term perfusion of microvascular networks with or without circulating cells at physiological levels of flow. The low dead volume allows for adequate buildup of secreted factors, such as cytokines.

Imaging of MVNs, average morphological analysis, permeability assay, and perfusability assessment

MVNs were imaged using either an Olympus FV1000 (Olympus, Japan) confocal laser scanning microscope or a Nikon Eclipse Ti epifluorescence microscope (Nikon, Japan). Epifluorescent images of the MVNs were acquired using the 4× objective. Morphological analysis was performed in Image J (NIH) by thresholding the MVN signal using Trainable Weka Segmentation, measuring the area of the MVNs, skeletonizing the MVN, and analyzing the skeleton using "Analyze Skeleton". Average MVN diameter was then calculated as

$$MVN_{avg.vessel\ diameter} = (vessel\ area)/(number\ of\ vessels * average\ vessel\ length). \tag{2}$$

Permeability of MVNs under static conditions was measured by aspirating medium from the device media channels and introducing 100 μL of 0.1 mg mL^{-1} 70 kDa Texas Red dextran (Thermo Fischer Scientific). For flow-conditioned samples connected to the pump, 100 μL of 0.1 mg mL^{-1} 70 kDa Texas Red dextran (Thermo Fischer Scientific) was added to the downstream media reservoir, the pump was manually actuated twice to flow in the dextran, and the excess fluid from the upstream reservoir was aspirated. Then, the change in intravascular and extravascular fluorescence intensity was quantified, as previously described[65]. Confocal z-stacks were acquired every 12 min using the confocal microscope with the 10× objective at 640 px resolution and 5 μm steps in the z-direction. The change in fluorescence intensity was analyzed using an ImageJ (NIH) macro and subsequently calculated using an established relationship as previously described[65]. MVN perfusability was assessed by introducing the same volume and concentration of 70 kDa Texas Red dextran as previously described (100 μL at 0.1 mg mL^{-1}), and visualizing the networks using an epifluorescence microscope. The vascular region was analyzed using three distinct regions of interest (ROIs) imaged with a 4× objective. The dextran signal was compared to the BFP-HUVEC signal to evaluate perfusability. Each ROI was scored as 0 (not perfusable), 1 (partially perfusable), or 2 (fully perfusable), resulting in a total MVN score ranging from 0 to 6 when all ROI scores were summed. This total score was then divided by 6 to yield the perfusable area fraction.

Computational fluid transport model for morphological analysis and velocity, flow rate, and WSS calculations

The micro-Vascular Evaluation System (μVES)[16] was used as the computational model. μVES was used to calculate the flow rate, velocity, and WSS across every individual MVN segment. Flow rate boundary conditions were determined based on the experimentally measured MVN hydraulic resistances and corresponding flow rates. Maximum projected, 2D thresholded images were used as input to μVES. A custom vessel perturbation algorithm was added to μVES and used to conduct a vessel radius perturbation analysis. For the vessel perturbation study, the diameter of one vessel segment of interest was decreased by 10%, the complete MVN flow simulation was re-run using the same boundary conditions, and the WSS, velocity, flow rate, and diameter of the perturbed vessel segment was noted. This same procedure was done for each vessel segment of interest, perturbing one vessel segment at a time while keeping the diameters of the remaining MVN unperturbed. The derivative of the flow property (ie. WSS, flow rate, or velocity) with respect to the derivate of the radius was calculated as

$$\frac{d(\{WSS, flow\ rate, velocity\})}{dr} = \frac{\{WSS, flow\ rate, velocty\}_{original} - \{WSS, flow\ rate, velocty\}_{perturbed}}{r_{original} - r_{perturbed}}, \tag{3}$$

where r is the vessel radius.

Inflammatory cytokine analysis

The full volume of conditioned media (200 μL) was collected from static devices on day 7, 9, and 11, and from long-term flow devices on day 9, 11, 14 and 22 and used in a Human Focused 15-Plex Discovery Assay® (Eve Technologies). For the transwell system, 500 μL of the conditioned medium from the transwell insert was collected and used in the same Human Focused 15-Plex Discovery Assay® (Eve Technologies). For all conditions, the medium was in contact with the MVNs for 24 h before sampling. Samples of growth medium and maintenance medium were also analyzed for background signal, which was subtracted from all conditioned medium samples. A subset of static devices after day 7 sampling were then connected to the pump for long-term flow follow up on days 14 and 22, as previously described. Fresh media was added to the long-term flow devices and pump flow was resumed.

Bulk RNA sequencing

For each timepoint analyzed, the fibrin hydrogel containing the MVNs was cut out of the devices and placed in 5 mL of 100 μg mL^{-1} Liberase (Millipore Sigma), 100 μg mL^{-1} DNase I (Sigma Aldrich), and 9.2 μg mL^{-1} Elastase (Thermo Fischer Scientific) in DMEM (Thermo Fischer Scientific) for 75 min at 37 °C with intermittent agitation. Cells from 3 to 4 devices were pooled for each replicate. Dead cells were removed using the Dead Cell Removal Kit and an OctoMACS Separator (Miltenyi Biotec), cells were incubated with CD31 MicroBeads (CD31 MicroBead Kit, Miltenyi Biotec) and HUVECs and FBs were sorted using the OctoMACS Separator (Miltenyi Biotec). The sorted cells were lysed with TRIzol (Thermo Fischer) and stored at −80 °C. Once the cell lysates from all timepoints were collected, the lysates were thawed, and 0.2 mL of chloroform (Millipore Sigma) per 1 mL of TRIzol reagent was added, the samples were centrifuged for 15 min at 12,000 × g at 4 °C, and the aqueous phase was collected. The samples were then prepared using the "Preparation of Cell Pellets" protocol for RNA extraction using the

chemagic 360 (Revvity). RNA quality and concentration was confirmed using a Fragment Analyzer (Agilent BioSciences). RNAseq libraries were generated from 20 ng of totalRNA using NEBNext UltraII Directional RNA library prep kit (New England Biolabs) using a 1/5 reaction volume on the SPT Mosquito HV (Mildum et al., JBT 2020). Libraries were amplified using Singular S1/S2 anchor sequences and sequencing on a Singular G4 F3 flowcell (Singular Genomics) using 50nt paired end sequencing. RNA-seq data analysis was conducted using a robust R-based pipeline. BAM files were quantified with featureCounts[66] to generate a counts matrix, which was processed with DESeq2[67] for differential gene expression analysis. Genes with low expression were filtered out, and more than four biological replicates per condition ensured statistical rigor. PCA confirmed sample clustering by condition. Pathway enrichment analysis was performed using clusterProfiler[68], identifying significantly enriched pathways that contextualize the observed gene expression changes. The R code used for analyzing the counts files has been uploaded to the repository.

Mass spectrometry

Digestion of tissue samples into peptides was performed using previously published methods[69] for mass spectrometry-based proteomics, and were optimized to identify ECM-related proteins[70]. Briefly, the tissue was first decellularized, then reduction with DTT, deglycosylation with PNGaseF, digestion with Lys-C and trypsin, and acidification with trifluoro-acetic acid were performed according to the published protocol[70]. Peptides desalting using Protea C18 spin tips, lyophilization, and labeling with TMT 10plex (Thermo) was performed per manufacturer's instructions. Additionally, peptides were separated by reverse phase HPLC (Thermo Easy nLC1000) using a precolumn (made in house, 6 cm of 10 µm C18) and a self-pack 5 µm tip analytical column (12 cm of 5 µm C18, New Objective) over a 140-min gradient before nanoelectrospray using a QExactive Plus mass spectrometer (Thermo). Raw mass spectral data files (.raw) were searched using Proteome Discoverer (Thermo) and Mascot version 2.4.1 (Matrix Science). TMT quantification was obtained using Proteome Discoverer and isotopically corrected per manufacturer's instructions. Matrix proteins were determined as previously defined[70]. To identify unique groupings of temporal protein deposition, fold change increase was calculated for each protein during each of the 3 intervals (D1-D4, D4-D7, D7-D14). First, the proteins were divided into 2 groups based on fold change above or below the average for interval 1. Those groups were then subdivided based on fold change above or below the average for interval 2. Finally, those groups were subdivided based on the fold change above or below the average for interval 3. Relative protein abundance was calculated using the Top-3 method. Briefly, of all identified peptides mapping to a given protein, those with the largest 3 precursor areas were averaged together and used as the abundance parameter for that protein. The abundance parameter for each protein was divided by the sum of abundance parameters for all proteins to determine its relative abundance.

Statistics

Average values are reported as mean ± standard deviation and sample sizes are reported in figure legends. Statistical analysis was performed using GraphPad Prism software, version 10. Parametric, two-tailed t tests were applied to analyses involving two groups and ordinary one-way ANOVA with Tukey's multiple comparison tests were applied to analyses involving more than two groups. Experiments consisting of tracking the same MVNs over time used paired statistics. For the 2D analysis group separation analysis, the Henze–Zirkler test statistic was used to test for normality and a 2D permutation test with 10,000 permutations was used to as the test statistic. The random seed was set to 101 for all groups compared. A 2D group separation analysis using linear discriminant analysis was used to find a linear decision boundary between two groups in the 2D comparison. * indicates $p < 0.05$, ** indicates $p < 0.01$, *** indicates $p < 0.001$, **** indicates $p < 0.0001$, and n.s. indicates $p > 0.05$.

Data availability

All the data/metadata generated in support of the reported findings can be found at Fairdomhub: https://fairdomhub.org/studies/1337. The SRA/GEO Submission is associated with bioproject: https://www.ncbi.nlm.nih.gov/sra/PRJNA1248549.

Received: 6 December 2024; Accepted: 3 September 2025;
Published online: 04 November 2025

References

1. Pober, J. S. & Sessa, W. C. Inflammation and the blood microvascular system. *Cold Spring Harb. Perspect. Biol.* **7**, a016345 (2015).
2. McDONALD, D. M. Angiogenesis and remodeling of airway vasculature in chronic inflammation. *Am. J. Respir. Crit. Care Med.* **164**, S39–S45 (2001).
3. Whiteford, J. R., De Rossi, G. & Woodfin, A. Mutually supportive mechanisms of inflammation and vascular remodeling. In *International Review of Cell and Molecular Biology* vol. 326 201–278 (Elsevier, 2016).
4. Whisler, J. et al. Emergent mechanical control of vascular morphogenesis. *Sci. Adv.* **9**, eadg9781 (2023).
5. Chen, M. B. et al. On-chip human microvasculature assay for visualization and quantification of tumor cell extravasation dynamics. *Nat. Protoc.* **12**, 865–880 (2017).
6. Nguyen, H. T. et al. Patient-specific vascularized tumor model: blocking TAM recruitment with multispecific antibodies targeting CCR2 and CSF-1R. *Biomaterials.* **213**, 122731 (2025).
7. Wan, Z. et al. New strategy for promoting vascularization in tumor spheroids in a microfluidic assay. *Adv. Healthc. Mater.* **12**, 2201784 (2023).
8. Wan, Z. et al. Transmural flow upregulates PD-L1 expression in microvascular networks. *Adv. Sci.* **11**, 2400921 (2024).
9. Cherubini, M. et al. Flow in fetoplacental-like microvessels in vitro enhances perfusion, barrier function, and matrix stability. *Sci. Adv.* **9**, eadj8540 (2023).
10. Haase, K. et al. Physiologic flow-conditioning limits vascular dysfunction in engineered human capillaries. *Biomaterials* https://doi.org/10.1101/2021.03.03.433247 (2021).
11. Blazeski, A. et al. Engineering microvascular networks using a KLF2 reporter to probe flow-dependent endothelial cell function. *Biomaterials* **311**, 122686 (2024).
12. Davies, P. F. Hemodynamic shear stress and the endothelium in cardiovascular pathophysiology. *Nat. Clin. Pract. Cardiovasc. Med.* **6**, 16–26 (2009).
13. Offeddu, G. S. et al. Microheart: A microfluidic pump for functional vascular culture in microphysiological systems. *J. Biomech.* **119**, 110330 (2021).
14. Bourquin, C., Poree, J., Lesage, F. & Provost, J. In vivo pulsatility measurement of cerebral microcirculation in rodents using dynamic ultrasound localization microscopy. *IEEE Trans. Med. Imaging* **41**, 782–792 (2022).
15. Kheiri, S. et al. Integrating spheroid-on-a-chip with tubeless rocker platform: a high-throughput biological screening platform. *Biotechnol. J.* **18**, 2200621 (2023).
16. Rota, A. et al. A three-dimensional method for morphological analysis and flow velocity estimation in microvasculature on-a-chip. *Bioeng. Transl. Med.* **8**, e10557 (2023).
17. Hamilton, J. A. GM-CSF in inflammation. *J. Exp. Med.* **217**, e20190945 (2020).
18. Libby, P. Inflammation in atherosclerosis. *Nature* **420**, 868–874 (2002).
19. Apostolakis, S., Vogiatzi, K., Amanatidou, V. & Spandidos, D. A. Interleukin 8 and cardiovascular disease. *Cardiovasc. Res.* **84**, 353–360 (2009).
20. Carbone, M. L. & Failla, C. M. Interleukin role in the regulation of endothelial cell pathological activation. *Vasc. Biol.* **3**, R96–R105 (2021).

21. Gabay, C. Interleukin-6 and chronic inflammation. *Arthritis. Res. Ther.* **8**, S3 (2006).
22. Bui, T. M., Wiesolek, H. L. & Sumagin, R. ICAM-1: A master regulator of cellular responses in inflammation, injury resolution, and tumorigenesis. *J. Leukoc. Biol.* **108**, 787–799 (2020).
23. Lawson, C. & Wolf, S. ICAM-1 signaling in endothelial cells. *Pharmacol. Rep.* **61**, 22–32 (2009).
24. Cook-Mills, J. M., Marchese, M. E. & Abdala-Valencia, H. Vascular cell adhesion molecule-1 expression and signaling during disease: regulation by reactive oxygen species and antioxidants. *Antioxid. Redox Signal.* **15**, 1607–1638 (2011).
25. Psefteli, P.-M., Fowler, M., Draijer, R., Mann, G. E. & Siow, R. Role of the glycocalyx in fluid shear stress modulation of heme oxygenase-1 in human endothelial cells. *Free Radic. Biol. Med.* **100**, S148 (2016).
26. Psefteli, P.-M. et al. Glycocalyx sialic acids regulate Nrf2-mediated signaling by fluid shear stress in human endothelial cells. *Redox Biol.* **38**, 101816 (2021).
27. Blanchard, N. et al. Dichotomous role of integrin-β5 in lung endothelial cells. *Pulm. Circ.* **12**, e12156 (2022).
28. Wu, J. et al. Neuroprotective effects of sulfiredoxin-1 during cerebral ischemia/reperfusion oxidative stress injury in rats. *Brain Res. Bull.* **132**, 99–108 (2017).
29. Li, X. et al. Sulfiredoxin-1 enhances cardiac progenitor cell survival against oxidative stress via the upregulation of the ERK/NRF2 signal pathway. *Free Radic. Biol. Med.* **123**, 8–19 (2018).
30. Gautheron, J. & Jéru, I. The multifaceted role of epoxide hydrolases in human health and disease. *Int. J. Mol. Sci.* **22**, 13 (2020).
31. Pei, J., Pan, X., Wei, G. & Hua, Y. Research progress of glutathione peroxidase family (GPX) in redoxidation. *Front. Pharmacol.* **14**, 1147414 (2023).
32. Karpinich, N. O., Hoopes, S. L., Kechele, D. O., Lenhart, P. M. & Caron, K. M. Adrenomedullin function in vascular endothelial cells: insights from genetic mouse models. *Curr. Hypertens. Rev.* **7**, 228–239 (2011).
33. Rajan, A. M., Ma, R. C., Kocha, K. M., Zhang, D. J. & Huang, P. Dual function of perivascular fibroblasts in vascular stabilization in zebrafish. *PLOS Genet* **16**, e1008800 (2020).
34. Guillard, J. & Schwörer, S. Metabolic control of collagen synthesis. *Matrix Biol.* **133**, 43–56 (2024).
35. Offeddu, G. S. et al. Personalized vascularized models of breast cancer desmoplasia reveal biomechanical determinants of drug delivery to the tumor. *Adv. Sci.* **11**, 2402757 (2024).
36. Ko, E. C. et al. Accelerating the in vitro emulation of Alzheimer's disease-associated phenotypes using a novel 3D blood-brain barrier neurosphere co-culture model. *Front. Bioeng. Biotechnol.* **11**, 1251195 (2023).
37. Nishikata, K., Doi, K., Kaneoya, N., Nakamura, M. & Futai, N. In vitro model of vascular remodeling under microfluidic perfusion. *Micromachines*. **16**, 14 (2024).
38. Offeddu, G. Microphysiological endothelial models to characterize subcutaneous drug absorption. *ALTEX* https://doi.org/10.14573/altex.2207131 (2022).
39. Offeddu, G. S. et al. An on-chip model of protein paracellular and transcellular permeability in the microcirculation. *Biomaterials* **212**, 115–125 (2019).
40. Rodbard, S. Vascular caliber. *Cardiology* **60**, 4–49 (1975).
41. Kamiya, A. & Togawa, T. Adaptive regulation of wall shear stress to flow change in the canine carotid artery. *Am. J. Physiol. Heart Circ. Physiol.* **239**, H14–H21 (1980).
42. Qi, Y. et al. Hemodynamic regulation allows stable growth of microvascular networks. *Proc. Natl. Acad. Sci.* **121**, e2310993121 (2024).
43. Wagenseil, J. E. & Mecham, R. P. Vascular extracellular matrix and arterial mechanics. *Physiol. Rev.* **89**, 957–989 (2009).
44. Rucker, H. K., Wynder, H. J. & Thomas, W. E. Cellular mechanisms of CNS pericytes. *Brain Res. Bull.* **51**, 363–369 (2000).
45. Fitridge, R. & Thompson, M. *Mechanisms of Vascular Disease: A Reference Book for Vascular Specialists*. 13–24 (University of Adelaide Press, 2011).
46. Mill, P., Christensen, S. T. & Pedersen, L. B. Primary cilia as dynamic and diverse signalling hubs in development and disease. *Nat. Rev. Genet.* **24**, 421–441 (2023).
47. Vion, A.-C. et al. Primary cilia sensitize endothelial cells to BMP and prevent excessive vascular regression. *J. Cell Biol.* **217**, 1651–1665 (2018).
48. Szaba, F. M. & Smiley, S. T. Roles for thrombin and fibrin(ogen) in cytokine/chemokine production and macrophage adhesion in vivo. *Blood* **99**, 1053–1059 (2002).
49. Iannucci, J. & Grammas, P. Thrombin, a key driver of pathological inflammation in the brain. *Cells* **12**, 1222 (2023).
50. Tamargo, I. A., Baek, K. I., Kim, Y., Park, C. & Jo, H. Flow-induced reprogramming of endothelial cells in atherosclerosis. *Nat. Rev. Cardiol.* **20**, 738–753 (2023).
51. Gerszten, R. E. et al. MCP-1 and IL-8 trigger firm adhesion of monocytes to vascular endothelium under flow conditions. *Nature* **398**, 718–723 (1999).
52. Bickel, M. The role of interleukin-8 in inflammation and mechanisms of regulation. *J. Periodontol.* **64**, 456–460 (1993).
53. Haase, K., Gillrie, M. R., Hajal, C. & Kamm, R. D. Pericytes contribute to dysfunction in a human 3D model of placental microvasculature through VEGF-Ang-Tie2 signaling. *Adv. Sci.* **6**, 1900878 (2019).
54. Petreaca, M. L., Yao, M., Liu, Y., DeFea, K. & Martins-Green, M. Transactivation of vascular endothelial growth factor receptor-2 by interleukin-8 (IL-8/CXCL8) is required for IL-8/CXCL8-induced endothelial permeability. *Mol. Biol. Cell* **18**, 5014–5023 (2007).
55. Bussolino, F., Colotta, F., Bocchietto, E., Guglielmetti, A. & Mantovani, A. Recent developments in the cell biology of granulocyte-macrophage colony-stimulating factor and granulocyte colony-stimulating factor: activities on endothelial cells. *Int. J. Clin. Lab. Res.* **23**, 8–12 (1993).
56. Fahey, E. & Doyle, S. L. IL-1 family cytokine regulation of vascular permeability and angiogenesis. *Front. Immunol.* **10**, 1426 (2019).
57. Ito, A. et al. Degradation of interleukin 1β by matrix metalloproteinases. *J. Biol. Chem.* **271**, 14657–14660 (1996).
58. Zhang, T. et al. Open microfluidic coculture reveals paracrine signaling from human kidney epithelial cells promotes kidney specificity of endothelial cells. *Am. J. Physiol. Ren. Physiol.* **319**, F41–F51 (2020).
59. Carmeliet, P. & Jain, R. K. Angiogenesis in cancer and other diseases. *Nature* **407**, 249–257 (2000).
60. Sen-Banerjee, S. et al. Kruppel-like factor 2 as a novel mediator of statin effects in endothelial cells. *Circulation* **112**, 720–726 (2005).
61. Rojas-González, D. M., Babendreyer, A., Ludwig, A. & Mela, P. Analysis of flow-induced transcriptional response and cell alignment of different sources of endothelial cells used in vascular tissue engineering. *Sci. Rep.* **13**, 14384 (2023).
62. Helle, E., Ampuja, M., Antola, L. & Kivelä, R. Flow-induced transcriptomic remodeling of endothelial cells derived from human induced pluripotent stem cells. *Front. Physiol.* **11**, 591450 (2020).
63. Tanke, N. T. et al. Endothelial cell flow-mediated quiescence is temporally regulated and utilizes the cell cycle inhibitor p27. *BioRxiv Prepr. Serv. Biol*. https://doi.org/10.1101/2023.06.09.544403 (2024).
64. Wan, Z. et al. A robust vasculogenic microfluidic model using human immortalized endothelial cells and Thy1 positive fibroblasts. *Biomaterials* **276**, 121032 (2021).
65. Hajal, C. et al. Engineered human blood–brain barrier microfluidic model for vascular permeability analyses. *Nat. Protoc.* **17**, 95–128 (2022).
66. Liao, Y., Smyth, G. K. & Shi, W. featureCounts: an efficient general purpose program for assigning sequence reads to genomic features. *Bioinformatics* **30**, 923–930 (2014).
67. Love, M. I., Huber, W. & Anders, S. Moderated estimation of fold change and dispersion for RNA-seq data with DESeq2. *Genome Biol.* **15**, 550 (2014).

68. Xu, S. et al. Using clusterProfiler to characterize multiomics data. *Nat. Protoc.* **19**, 3292–3320 (2024).
69. Naba, A., Clauser, K. R. & Hynes, R. O. Enrichment of extracellular matrix proteins from tissues and digestion into peptides for mass spectrometry analysis. *J. Vis. Exp.* **101**, e53057, https://doi.org/10.3791/53057 (2015).
70. Naba, A. et al. The matrisome: in silico definition and in vivo characterization by proteomics of normal and tumor extracellular matrices. *Mol. Cell. Proteom. MCP* **11**, M111.014647 (2012).

Acknowledgements

The authors are thankful to Charlie Demurjian for preparing the data for open access publishing, Stuart Levine for guidance in designing and executing experiments for bulk RNA sequencing, Luca Possenti and Alberto Rota for troubleshooting the μVES code. M.F. was supported by an MIT MathWorks Fellowship. E.C. was supported by an Early Postdoc.Mobility fellowship from the Swiss National Science Foundation (P2EZP2_199914), a postdoctoral fellowship from the Ludwig Center at MIT Koch Institute for Integrative Cancer Research, and a Postdoc.Mobility fellowship from the Swiss National Science Foundation (P500PB_222131). This work was supported by a grant from the National Cancer Institute (U54-CA261694). The funder played no role in study design, data collection, analysis and interpretation of data, or the writing of this manuscript.

Author contributions

M.F. performed all experiments and analyzed the data. M.F., A.B., G.O. designed and performed conceptual flow experiments. M.F., E.C., M.F.C., Z.W. designed the long-term flow experiments and contributed to the writing and editing of the manuscript. V.V. and A.K. performed the RNAseq analysis. J.W. performed the proteomics and mass spectrometry experiments and analysis. All authors reviewed and/or edited the manuscript before submission.

Competing interests

R.D.K. is a co-founder of AIM Biotech, a company that markets microfluidic technologies and receives research support from Amgen, AbbVie, Boehringer-Ingelheim, GSK, Novartis, Roche, Takeda, Eisai, EMD Serono and Visterra. None of these activities is related to the content of this article. The other authors declare no competing interests. All other authors declare no financial competing interests.

Additional information

Supplementary information The online version contains supplementary material available at https://doi.org/10.1038/s44341-025-00028-0.

Correspondence and requests for materials should be addressed to Roger D. Kamm.